3b2 Version Number : 7.51c/W (Jun 11 2001)
File path : p:/Santype/Journals/Taylor&Francis/Unht/v52n3/unht214929/unht214929.3d
Date and Time : 23/6/07 and 19:59

Numerical Heat Transfer, Part A, 52: 1–16, 2007

ISSN: 1040-7782 print/1521-0634 online
DOI: 10.1080/00397910601150007

Taylor & Francis
Taylor & Francis Group

APPLICATION OF SMOOTHED PARTICLE HYDRODYNAMICS METHOD TO FREE SURFACE AND SOLIDIFICATION PROBLEMS

Mingyu Zhang, Hui Zhang, and Lili Zheng
Department of Mechanical Engineering, State University of New York at Stony Brook, Stony Brook, New York, USA

The smoothed particle hydrodynamics (SPH) method is developed to simulate free surface and solidification problems. A new treatment is included to handle particles near the free and solidification interfaces. The method is applied to a droplet impacting on substrates with different roughnesses. Spreading, solidification, oxide redistribution, and droplet pinch-off are presented in two- and three-dimensional geometry configurations. This work demonstrates the SPH model as a powerful tool to study transport phenomena in problems with free surface deformation and solidification.

1. INTRODUCTION

Thermal spray is a continuous, direct melt-spray process in which particles of virtually any materials are melted and accelerated to high velocities. The molten or semimolten droplets impinge on a substrate and solidify rapidly to form thin "splats." The deposit is built up by successive impingement and interbonding among the splats to form a well-bonded deposit. The primary advantages of this process are (1) its versatility with respect to gun and feed materials, (2) the capacity to form barrier and functional coatings on a wide range of substrates, and (3) the ability to create free-standing structures for net-shape manufacturing of high-performance ceramics, composites, and functionally graded materials [1–4].

Spreading and solidification of molten droplets are the key processes in thermal spray coating. They are also crucial for soldering, inkjet, and many other types of materials processing. When a molten droplet is in contact with a cold substrate or previously deposited splats, a high rate of heat transfer from the droplet to the substrate leads to a significant melt undercooling near the substrate. Crystalline nuclei form on the substrate surface, which is followed, most of the time, by columnar growth. Depending on heat transfer and solidification conditions, either planar or cellular nuclei or both may be possible during solidification, leading to very different microstructures. An interface tracking scheme is usually required to obtain an accurate solution. Numerical investigations undertaken so far have been based on

Received 18 April 2006; accepted 18 November 2006.
This work is supported by the National Science Foundation through DMR MRSEC-0080021.
Address correspondence to Mingyu Zhang, Department of Mechanical Engineering, State University of New York at Stony Brook, Stony Brook, NY 11794-2300, USA. E-mail: mizhang@ic.sunysb.edu

NOMENCLATURE

c	sound speed, m/s	s	interface position, m
C_p	specific capacity, J/kg K	t	time, s
d	spatial dimension	$\vec{v}$	particle velocity vector, m/s
D	parameter in Lennard-Jones form	V	velocity scale, m/s
f	repulsive force, kg m/s^2	W	smoothing function, m^{-3}
F	body force per unit mass, kg m/s^2	α_d	spatial coefficient
Fr	Froude number ($=gh/V_0^2$)	δ	density variation
h	smoothing length, m	$\delta^{\alpha\beta}$	unit tensor
Ja	Jakob number [$=C_p(T_f - T_{si})/h_{fs}$]	$\varepsilon^{\alpha\beta}$	shear strain rate, kg/m s^2
k	thermal conductivity, W/m K	μ	viscosity coefficient, kg/m s
L	length scale, m	ρ	particle density, kg/m^3
m	particle mass, kg	∇	gradient operator
p	pressure, kg/m s^2		
Pr	Prandtl number ($=\nu/\alpha$)	**Subscript**	
r	particle position, m	i, j	particle index
r_0	cutoff distance, m	l	liquid
Ra	roughness average, m	s	solid
Re	Reynolds number ($=\rho Vh/\mu$)	0	reference quantity

meshed methods, such as the volume-of-fluid (VOF) method [5–7], the level set method (LSM) [8, 9], and the deformable finite-element method (FEM) [10, 11]. Since the droplet impact involves large deformation of the free surface and moving solidification front, and sometimes the droplets splash, it is very difficult for a meshed method to track both moving interfaces. When pinch-off happens, the deformable FEM is no longer useful. Although the VOF method and the LSM can still be employed, the accuracy and stability of numerical schemes are questionable. To avoid the complications arising from large deformation and splashing, one of the mesh-free or meshless methods, smoothed particle hydrodynamics (SPH), will be employed in this article to study droplet spreading and solidification.

As one of the earliest mesh-free methods, the SPH method was developed in 1977 specifically to simulate phenomena in astrophysics [12, 13] and later applied to other fields [14–16]. The SPH method has been extended to many important applications related to fluid dynamics [17]. In the SPH method, the continuum medium is represented by a discrete set of particles, each with a given mass and velocity, and the macroscopic field equations are represented by particle dynamics which are different from the traditional meshed methods. The particle interactions are simulated using either potential or weight functions. Since the SPH method uses smoothed particles as interpolation points to represent materials at discrete locations,it can easily trace material interfaces and moving boundaries. The smoothing function is the most important part of the SPH method, as it characterizes the behavior and performance of the particle interpolation. In the early studies, the Gaussian function was commonly used as the smoothing function. Later, various smoothing functions were devised, and some of them are approximations to the Gaussian function.

Due to the adaptive nature of the particle interpolation, the SPH method can handle large deformation and interface movement naturally. It is similar to the molecular dynamics method but is used in macroscopic fluid dynamics simulation. Morris [18]

used the SPH method to simulate surface tension acting on an interface between two fluids and demonstrated the interface deformation with similar density and viscosity of two fluids. The method is, however, difficult to extend to high density and viscosity ratios of two fluids, such as water and air. Nugent [19] applied the SPH method to van der Waals (vdW) fluid and studied the effects of surface tension on the oscillation of a droplet with an initial rectangular shape. Although the surface tension given by this method agreed well with the analytical solution, there are nonphysical particles clustering in the simulation. Meleán [20] improved the method of Nugent and removed the tensile instability by adding an artificial viscous force and an energy-generation term to the standard SPH equations. Meleán [21] used the SPH method to simulate the coalescence of colliding van der Waals liquid drops and considered the effects of different impact velocities on the collision of two drops. These simulations were performed only for low-energy collisions. Unfortunately, the new method by Meleán had to compromise between avoiding the tensile instability and reproducing the van der Waals phase diagram. Further, Monaghan [22] extended the SPH method to solve problems involving solidification and melting. Up to now, the most complex problems that have been studied by the SPH method are the fluid flow with either free surface or solidification. No study has been performed for problems involving both free surface and solidification movements. To simulate droplet deformation and solidification in thermal spray or inkjet applications, the numerical model should be capable of handling the interaction of surface deformation and solidification.

In this article, the SPH method is for the first time introduced to solve droplet spreading and solidification problems. New treatment is developed to handle the particles near the free surface and at the solidification interface. Two- and three-dimensional spreading, solidification, oxide redistribution, and droplet pinch-off or splashing are presented, and the effects of rough substrate and solidification on spreading are investigated. Also, multidrop impact is simulated by the improved SPH model to demonstrate the SPH model as a powerful tool for studying transport phenomena in droplet spreading and solidification.

2. SPH EQUATIONS FOR FLUID FLOW AND SOLIDIFICATION

In the SPH method, the continuum fluid is represented by many particles; the connectivity through elements or control volumes in the finite-element/finite-volume method is replaced by dynamic nearest-neighbor search; and spatial derivatives are handled by smoothing kernels, W_{ij}, as basis functions. To develop a SPH model for droplet deformation and solidification, the Navier-Stokes equations should be represented in the Lagrangian form instead of the traditional Eulerian form in the meshed methods. The Navier-Stokes equations for an incompressible fluid in the moving Lagrangian frame take the following forms:

$$\frac{D\rho}{Dt} = -\nabla \cdot \vec{u} = -\rho \frac{\partial u^{\beta}}{\partial x^{\beta}} \tag{1}$$

$$\frac{Du^{\alpha}}{Dt} = -\frac{1}{\rho}\frac{\partial p}{\partial x^{\alpha}} + \mu \frac{\partial \varepsilon^{\alpha\beta}}{\partial x^{\beta}} + g^{\alpha} \tag{2}$$

where ρ, u, and p represent fluid density, velocity, and pressure, respectively.

$$\varepsilon^{\alpha\beta} = \frac{\partial u^{\beta}}{\partial x^{\alpha}} + \frac{\partial u^{\alpha}}{\partial x^{\beta}} - \frac{2}{3}(\nabla \cdot \vec{u})\delta^{\alpha\beta}$$

is the shear strain rate, and g^{α} is the gravity force per unit mass. In order to describe the incompressible flow, it is necessary to use an artificial state equation to close the equation system. Based on the idea that a theoretically incompressible flow is practically compressible, Morris [23] introduced the artificial compressibility equation

$$p = c^2 \rho \tag{3}$$

where c is the speed of sound. The speed of sound should be large enough to guarantee small density variation. The speed of sound should be chosen according to the following rules:

$$c^2 \sim \frac{V_0^2}{\delta}, \qquad \frac{vV_0}{L_0\delta}, \qquad \frac{FL_0}{\delta} \tag{4}$$

where $\delta = \rho/\rho_0$, V_0 and L_0 are the reference velocity and length, respectively.

If the surface tension is not considered, the free shear stress condition is applied to the free surface. The movement of the solidification interface during droplet impact can be defined by satisfying the local energy balance. Assuming that the position of the interface can be expressed as $s(x, y, t) = 0$, the energy balance under the ideal conditions can have the following form [5]:

$$\frac{ds}{dt} = \frac{\mathrm{Ja}}{\mathrm{Re}\,\mathrm{Pr}} \frac{k_s}{k_l} \frac{1}{s} \tag{5}$$

where $\mathrm{Ja} = C_p(T_f - T_{si})/h_{fs}$ is the Jakob number, and h_{fs} is the latent heat. This equation has an analytical solution:

$$s = \sqrt{2\left(\frac{\mathrm{Ja}}{\mathrm{Re}\,\mathrm{Pr}} \frac{k_s}{k_l}\right) t} \tag{6}$$

The densities for liquid and solid are assumed to be constant and equal to each other. Since the purpose of this article is to demonstrate the capability of the SPH model in simulating a problem with both free surface and solidification interface movements, the simple solidification model is used. More complicated models can be applied after this work.

3. NUMERICAL FORMULATIONS OF THE SPH METHOD

The SPH method uses a particle interpolation method to calculate continuum field variables. The particles have mass, position, velocity, and other fluid quantities related to a specific problem. The SPH governing equations include interparticle forces and fluxes. The mass density ρ_i of the particle at position $\vec{r}_i$ can be evaluated as

$$\rho_i = \sum_j m_j W_{ij} \tag{7}$$

where $W_{ij} = W(\vec{x}_{ij}, h)$ is the smoothing function, and $\vec{x}_{ij} = \vec{x}_i - \vec{x}_j$, m_i denotes the mass of particle i, h represents the smoothing length and $\vec{x}_i$ is the position of particle i. Since the particles carry the mass, Eq. (7) conserves the total mass.

Applying the SPH particle approximation to the Lagrangian form of the Navier-Stokes equation, a symmetric form is obtained to preserve variational consistency. The dimensionless momentum equation in symmetric form is

$$\frac{Du_i^\alpha}{Dt} = -\sum_j m_j \left(\frac{p_i}{\rho_i^2} + \frac{p_j}{\rho_j^2}\right) \frac{\partial W_{ij}}{\partial x_i^\alpha} + \frac{1}{\mathrm{Re}} \sum_j m_j \left(\frac{\varepsilon_i^{\alpha\beta}}{\rho_i^2} + \frac{\varepsilon_j^{\alpha\beta}}{\rho_j^2}\right) \frac{\partial \mathrm{w}_{ij}}{\partial x_i^\beta} + \mathrm{Fr} \tag{8}$$

In Eq. (8), $\mathrm{Re}(=V_0 h/v)$ and $\mathrm{Fr}(=gh/V_0{}^2)$ are the Reynolds and Froude numbers, respectively, and $\varepsilon^{\alpha\beta}$ is the viscous strain rate, that is expressed as

$$\begin{aligned} \varepsilon_i^{\alpha\beta} = & \sum_j \frac{m_j}{\rho_j} u_{ij}^\beta \frac{\partial W_{ij}}{\partial x_i^\alpha} + \sum_j \frac{m_j}{\rho_j} u_{ji}^\alpha \frac{\partial W_{ij}}{\partial x_i^\beta} \\ & - \left(\frac{2}{3} \sum_j \frac{m_j}{\rho_j} \vec{u}_{ji} \cdot \nabla_i W_{ij}\right) \delta^{\alpha\beta} \end{aligned} \tag{9}$$

In the simulation, the SPH particle approximation is based on the cubic spline functions introduced by Monaghan and Lattanzio [24]. The function known as the B-spline function takes the form

$$W(S,h) = \alpha_d \times \begin{cases} \frac{2}{3} - S^2 + \frac{1}{2} S^3 & 0 \le S < 1 \\ \frac{1}{6}(2-S)^3 & 1 \le S < 2 \\ 0 & S \ge 2 \end{cases} \tag{10}$$

where $S = |\vec{x} - \vec{x}'|/h$ is the relative distance between two particles at the positions of $\vec{x}$ and x'. α_d takes the value of $15/7\pi h^2$ and $3/2\pi h^2$ for two and three dimensions, respectively. The B-spline function resembles a Gaussian function with a narrower compact support.

The following equation can be used to update the particle position:

$$\frac{d\vec{r}_i}{dt} = \vec{v}_i \tag{11}$$

According to the Courant–Friedrichs–Levy (CFL) condition, the time step is proportional to the smallest particle resolution:

$$\Delta t \sim \min\left(\frac{h_i}{c}\right) \tag{12}$$

The sound speed should be sufficiently small if a large time step is used.

The boundary of the computational domain is treated as virtual particles to exert repulsive force on fluid particles near the boundary. The repulsive force per

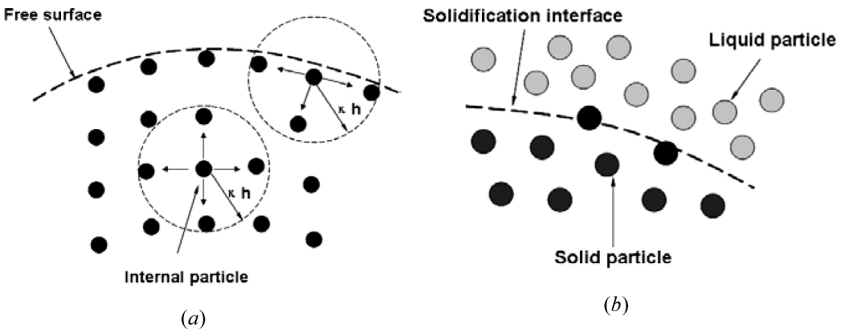

Figure 1. Schematics of the particles (*a*) near a free surface and (*b*) near a solidification interface in the SPH method.

unit mass $f(r)$ takes the form [25]:

$$f(r) = \begin{cases} D\left[\left(\frac{r_0}{r}\right)^{n_1} - \left(\frac{r_0}{r}\right)^{n_2}\right]\frac{\vec{r}}{r^2} & r \le r_0 \\ 0 & r \ge r_0 \end{cases} \tag{13}$$

where the parameters n_1 and n_2 take 12 and 4, respectively. The parameter D depends on the problem, and r_0 is the cutoff distance.

The free surface movement in droplet deformation can be simulated straightforwardly by using the SPH method if the surface tension is not considered. The effect of surface tension force can be neglected for a large droplet with millimeter-range size, while it is significant for a small droplet with micrometer-range size. It is proposed that the surface tension is simulated using the attractive forces among the particles near the free surface, as shown in Figure 1*a*. The forces acting on the internal particles will cancel out each other. The net force on each particle is perpendicular to the surface and centripetal only in a small strip around the free surface. The surface tension force can be incorporated into the current model in the future.

As pointed out by Monaghan [22], there exist some solid particles with mass smaller than liquid particles (Figure 1*b*). Monaghan avoids this problem by introducing solid particles without mass. The solid and liquid particles in this article are assumed to have the same mass. If the liquid particles are captured by the solidification interface, they will become solid particles. In the current model, the solidification movement is jumped. This treatment does not reflect the real situation. A new treatment to the solidification interface movement will be developed in the future in the particle method. The focus of this article is to evaluate the capability of SPH for both free surface and solidification interface movements.

4. RESULTS AND DISCUSSION

To demonstrate the applicability of the current SPH model, droplet spreading and solidification problems have been investigated. Since large deformation is involved in the droplet spreading with solidification along with complicated

interaction between free surface and solidification at the tri-phase boundary, it is extremely difficult to simulate this process using a meshed method. In thermal spraying, a layer of oxide is usually formed on the surface of a melt droplet as a result of in-flight oxidation. When a metal droplet impacts and spreads on the substrate, the oxide moves and remains following the movement of the free surface. It is important to understand the movement of oxide during impact, since it will significantly affect the thermal and mechanical properties of coatings. Such phenomena have been studied extensively in experiments. No model, however, is available to study this behavior. The roughness of the substrate plays an important role in droplet spreading. It is expected that the flattening degree will be hindered by the energy dissipation on the rough surface. Here, the SPH method is used to simulate the droplet spreading and solidification problem, as well as thermal sprayed coating with oxidation layer. The simulated problems are of great importance, but extremely difficult.

Figure 2 shows the schematic of a droplet impacting on a substrate in thermal spray. In the simulations, the radius of the droplet is assumed to be 1 mm. The droplet size is much larger than that of spray particles being injected. The surface tension of the droplet can be neglected in this article. For a smaller droplet, the surface tension force will be important. SPH particles of equal mass have uniform interparticle distance 50 μm in 2-D and 100 μm in 3-D simulation. The smoothing length is the same as the interparticle distance. Simulations have been performed to study the droplet impact on a smooth or rough substrate with $\mathrm{Re} = 10$ and $\mathrm{Fr} = 0.2$. Assuming that there exists an oxide layer on the free surface of the droplet, the force between oxide and molten metal particles is assumed to be the same as for internal metal particles. Different colors are assigned for different particles so that the movements of oxide particles can be traced. The time step used in the simulation is assumed to be 10 μs. The total numbers of particles used for a droplet in two and three dimensions are 1,249 and 3,828, respectively. The computer used in the simulations is a Pentium IV PC. The running times for 3,000 time steps in two and three dimensions are about 5 and 75 h, respectively. With optimized time steps, the running time can be reduced significantly. Six cases have been simulated, and results are presented next.

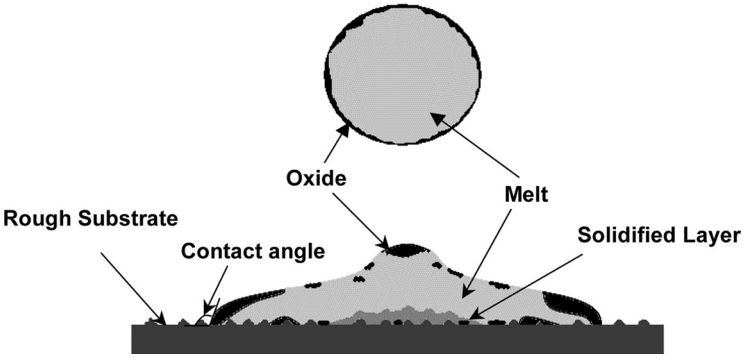

Figure 2. Schematic of a droplet impact.

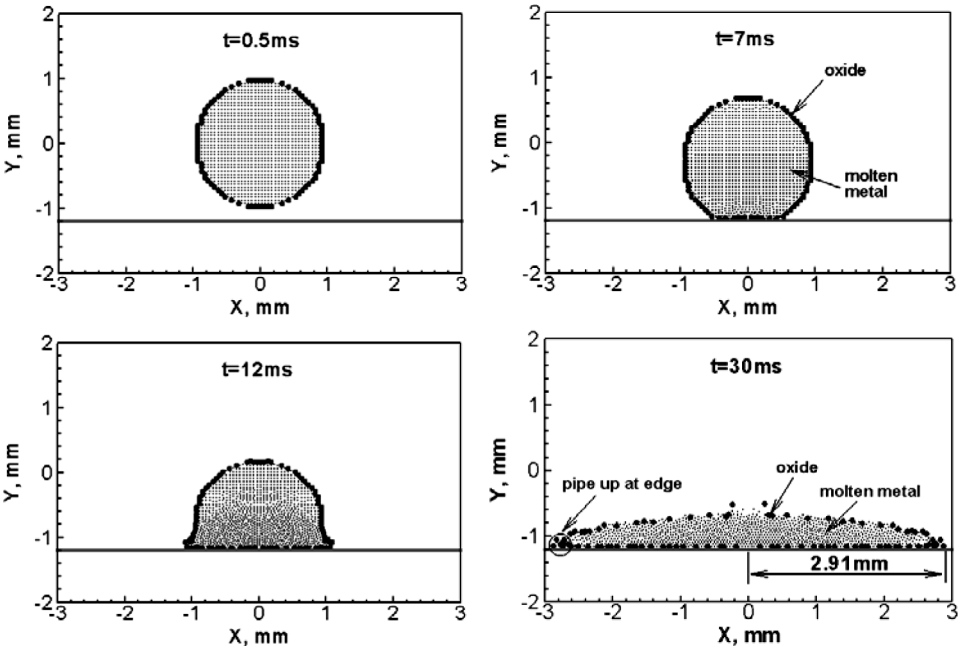

Figure 3. Droplet with oxide layer on the surface impacting on a smooth substrate for $\mathrm{Re} = 10$ and $\mathrm{Fr} = 0.2$ at $t = 0.5$, 7, 12, and 30 ms. The large black particles represent oxide and the small gray particles represent liquid.

Case 1: 2-D Droplet Impact on a Smooth Substrate

Figure 3 shows the time evolution of a metal droplet with an oxide layer spreading on a smooth substrate in two dimensions. When the droplet touches the substrate, it begins to deform. Because of the high pressure formed at the center of the impact region, the droplet will spread on the substrate. Initially the oxide layer has a uniform distribution on the droplet surface. Oxide at the upper surface moves with the liquid near the free surface and piles up in the region near the advancing front. The advancing contact angle in this case is greater than 90°. The predicted locations of oxides agree well with the experimental observation. This simulation demonstrates that the current SPH model can be used to simulate a large free surface deformation.

Case 2: 2-D Droplet Impact on a Rough Substrate

Single droplet impact on rough substrates with $\mathrm{Ra} = 62.5\,\mu\mathrm{m}$ (1/16 mm) and $\mathrm{Ra} = 100\,\mu\mathrm{m}$ (1/10 mm) are shown in Figures 4 and 5, respectively. The detachment of the droplet from the substrate and the free surface breakup occur at the outer edge when the droplet impacts on a rough substrate. Since computational particles can be assigned to any locations in the computational domain, the SPH method can be used to treat irregular geometry easily. Figure 4 shows the pore formation for the rough substrate with $\mathrm{Ra} = 100\,\mu\mathrm{m}$. The results confirm that the rough substrate will

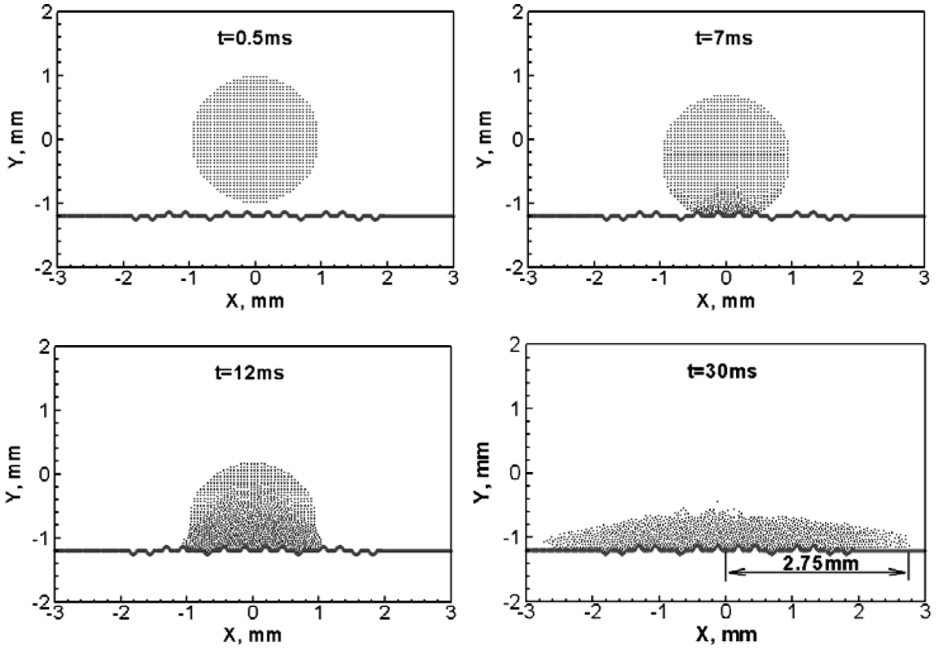

Figure 4. Droplet impacting on a rough substrate of Ra = 62.5 μm for Re = 10 and Fr = 0.2 at $t = 0.5$, 7, 12, and 30 ms.

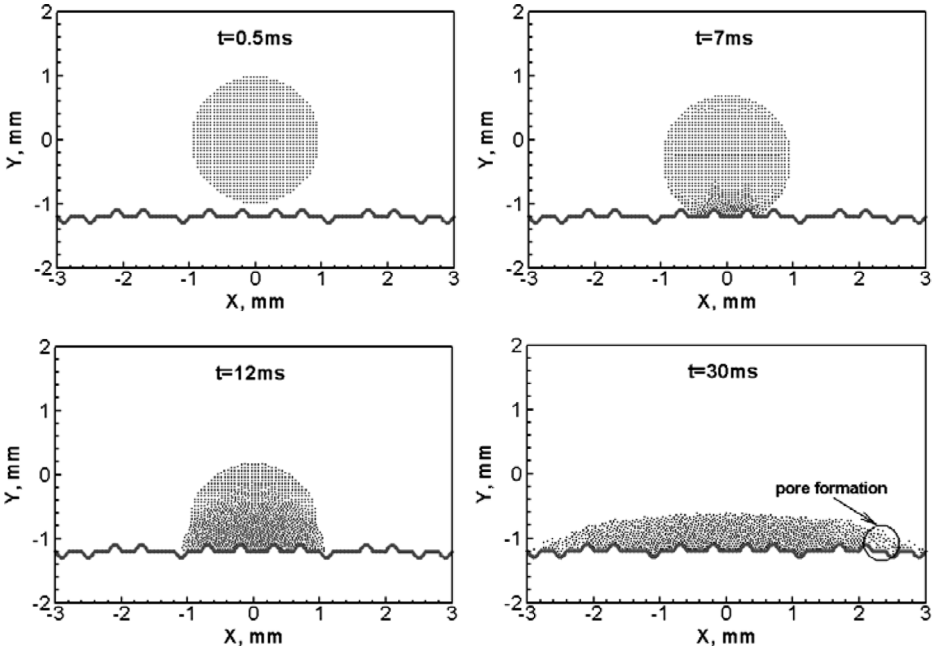

Figure 5. Droplet impacting on a rough substrate of Ra = 100 μm for Re = 10 and Fr = 0.2 at $t = 0.5$, 7, 12, and 30 ms.

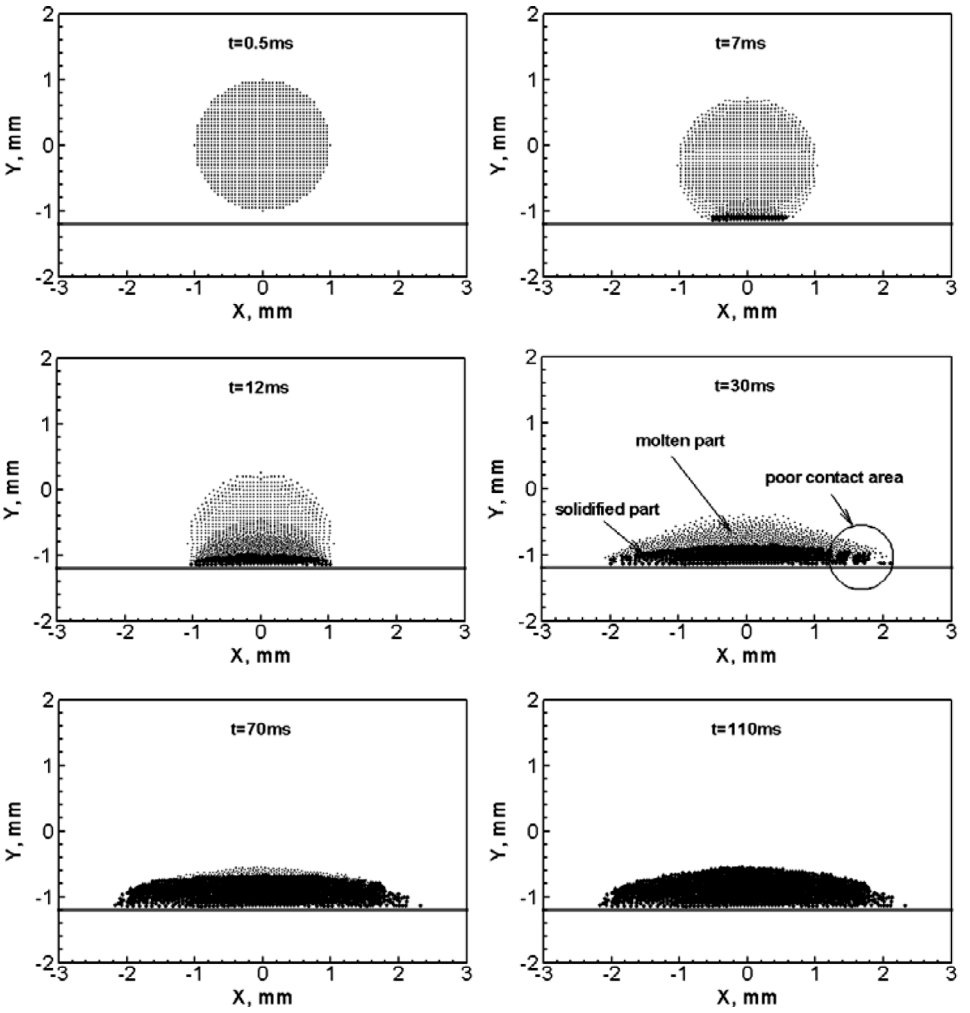

Figure 6. Droplet spreading and solidification on a cold substrate for Re = 10 and Fr = 0.2 at $t = 0.5$, 7, 12, 30, 70, and 110 ms. The large black particles represent solid and the small gray particles represent liquid.

cause droplet splashing. Under the simulated conditions, the maximum radius of the droplet spreading on the rough substrate is 2.75 mm at the time of 30 ms, which is smaller than that on a smooth substrate, 2.91 mm as shown in Figure 3. The rough substrate will increase the momentum dissipation and prevent the droplet from spreading.

Case 3: 2-D Droplet Spreading and Solidification

Figure 6 shows one set of results by the SPH method for solidification in the presence of free surface deformation. The prediction reveals that once the droplet reaches the cold substrate, the solidification interface moves upward and the droplet

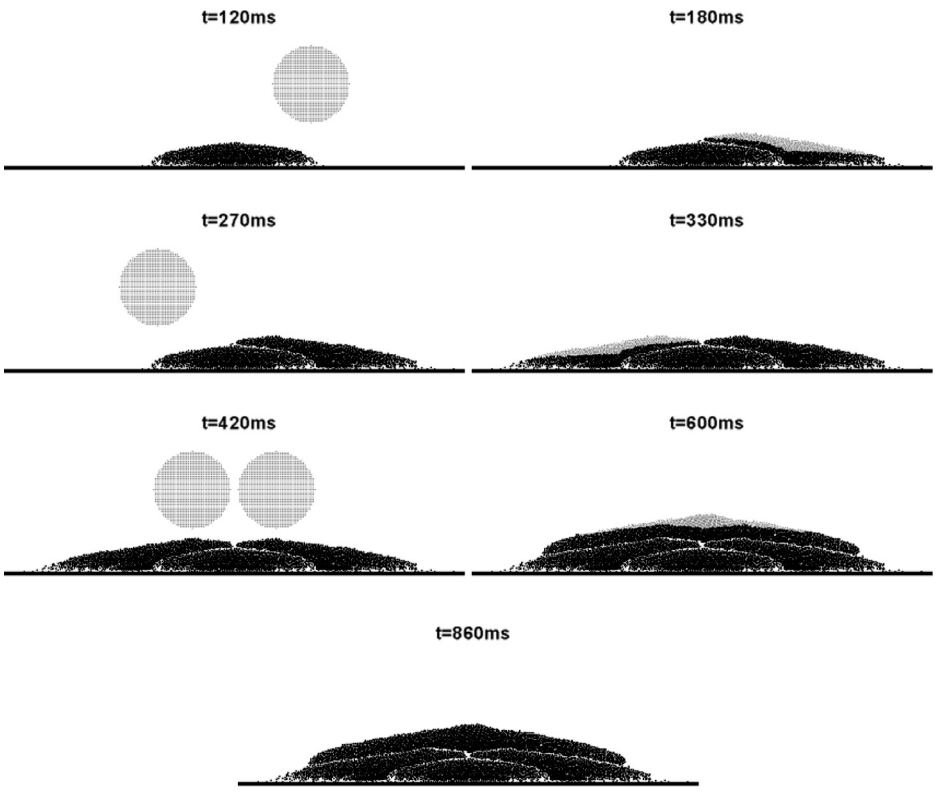

Figure 7. Five droplets impact and solidification on a cold substrate for Re = 10 and Fr = 0.2 at $t = 120$, 180, 270, 320, 420, 600, and 860 ms. The large black particles represent solid and the small gray particles represent liquid.

begins to solidify. At 12 ms, the liquid part of the splat deforms substantially. Initially the solidification interface moves upward quickly and captures many particles. After spreading is completed, the solidification interface moves slowly. This is due to the drop of temperature gradient. At 30 ms, the droplet spreads substantially. At 110 ms, the droplet solidifies completely. The contact between the drop and the substrate is good in the middle of the droplet, and it is poor at the edge of the droplet.

Case 4: Five Droplets Impact and Solidification

Since the SPH method can insert particles freely, it is convenient for the SPH method to simulate the interaction between multiple droplets and substrate. Spreading and solidification of five droplets are presented in Figure 7. The first three droplets impact one by one on a cold substrate at 0, 120, and 270 ms, respectively. The last two droplets impact on the substrate at the same time. The movement of the solidification interface is initially rapid due to the large temperature gradient, and then it gradually slows down. The solidification completes at 860 ms. At that time, poor

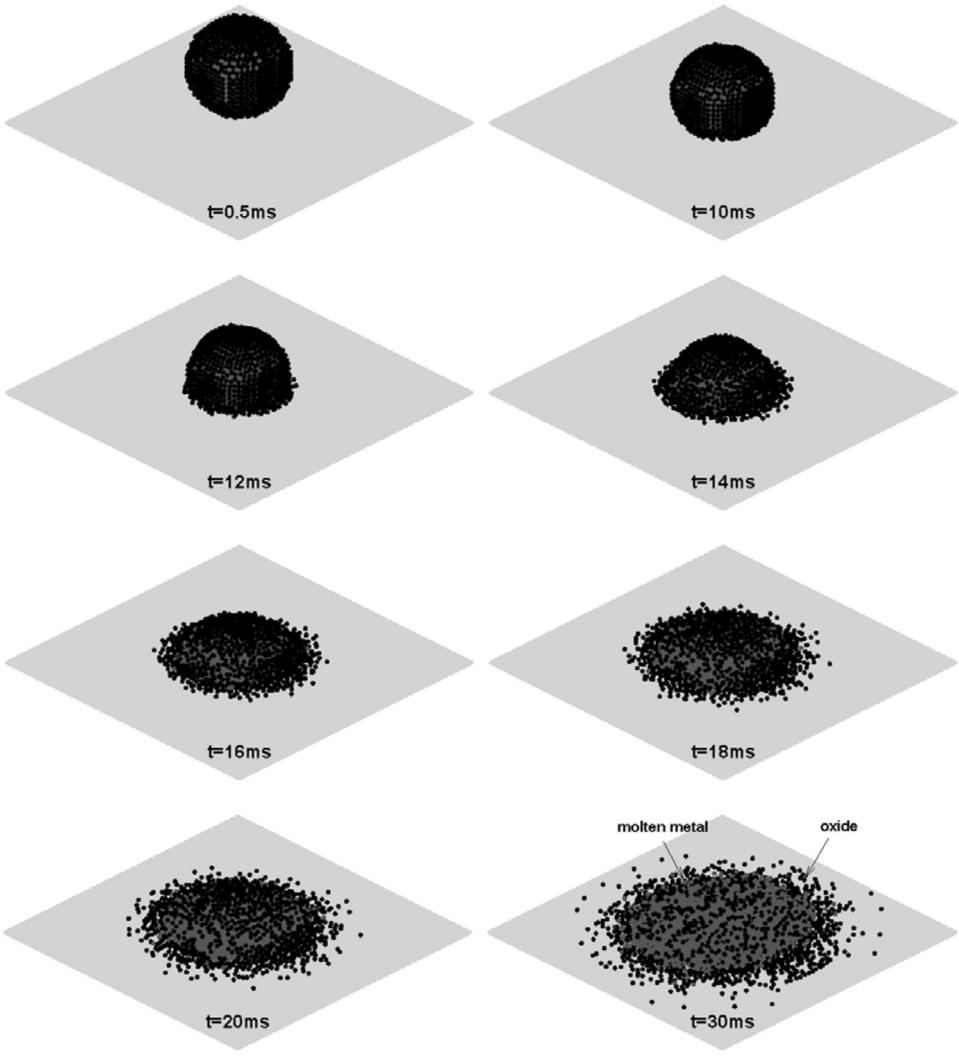

Figure 8. Droplet with oxide layer on the surface impacting on a smooth substrate for $\mathrm{Re} = 10$ and $\mathrm{Fr} = 0.2$ at $t = 0.5$, 10, 12, 14, 16, 18, 20, and 30 ms. The black particles represent oxide and the gray particles represent liquid.

contact is observed at the edges of the splats. Apparent boundaries exist between the splats.

Case 5: 3-D Droplet Impact and Oxide Redistribution

The 3-D SPH model is developed and used to simulate droplet deformation 265
with an oxide layer on the surface. The simulation results are shown in Figure 8. Due to the impact velocity and gravity force, the droplet deforms and spreads on

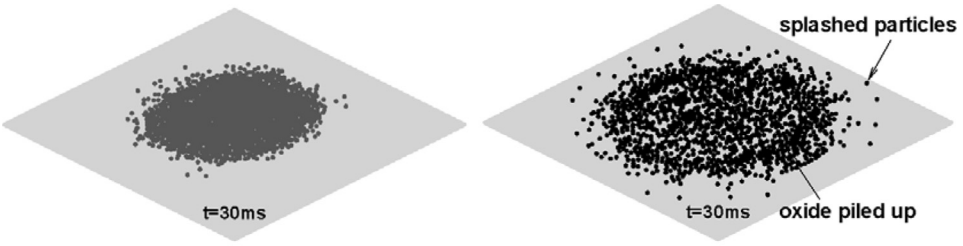

Figure 9. Droplet with oxide layer on the surface impacting on a smooth substrate for $\mathrm{Re} = 10$ and $\mathrm{Fr} = 0.2$ at $t = 30$ ms for (*a*) molten metal and (*b*) oxide, respectively. The black particles represent oxide and the gray particles represent liquid.

the substrate. The droplet deforms from its initial spherical shape to a cylindrical disk geometry. At 30 ms, the radius of the splat is about 3 mm, which agrees with 2-D results. Figure 9 shows a general view of the oxide distribution, and Figure 10 displays the oxide distribution on a specific cross section at $x = 0$. It is seen that the oxide is uniformly distributed on the droplet surface at the beginning. After impact, oxide particles move with the free surface and reside on the substrate or in the splat. At 30 ms, the initial spherical droplet converts into a flat splat. It is clear that oxide is piled up at the circumference of the splat to form a ring. The particles outside the ring are coming from splashing. The simulation results agree with experimental observation [26]. It is noted that simulating the splashing behavior in three dimensions is a difficult task using a meshed method. It is straightforward using the SPH method. The current simulation results again demonstrated the powerful capability of the SPH model.

Case 6: 3-D Droplet Spreading and Solidification

The current SPH model has also been used to investigate the interaction between the solidification interface and free surface in three dimensions. The results at 0, 8, 12, 16, 20, 30, 50, and 90 ms are shown in Figure 11. A quarter of the droplet has been taken out in order to show the movement of the solidification interface inside the droplet. It is seen that the droplet begins to solidify as soon as it touches the cold substrate. At the same time, droplet deformation occurs during impact. The spherical droplet deforms to form a splat with the shape of a cylindrical disk. There are some splashed particles around the edge.

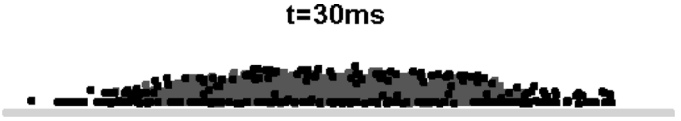

Figure 10. Oxide distribution on the cross section at $x = 0$ at $t = 30$ ms. The black and gray represent oxide and liquid, respectively.

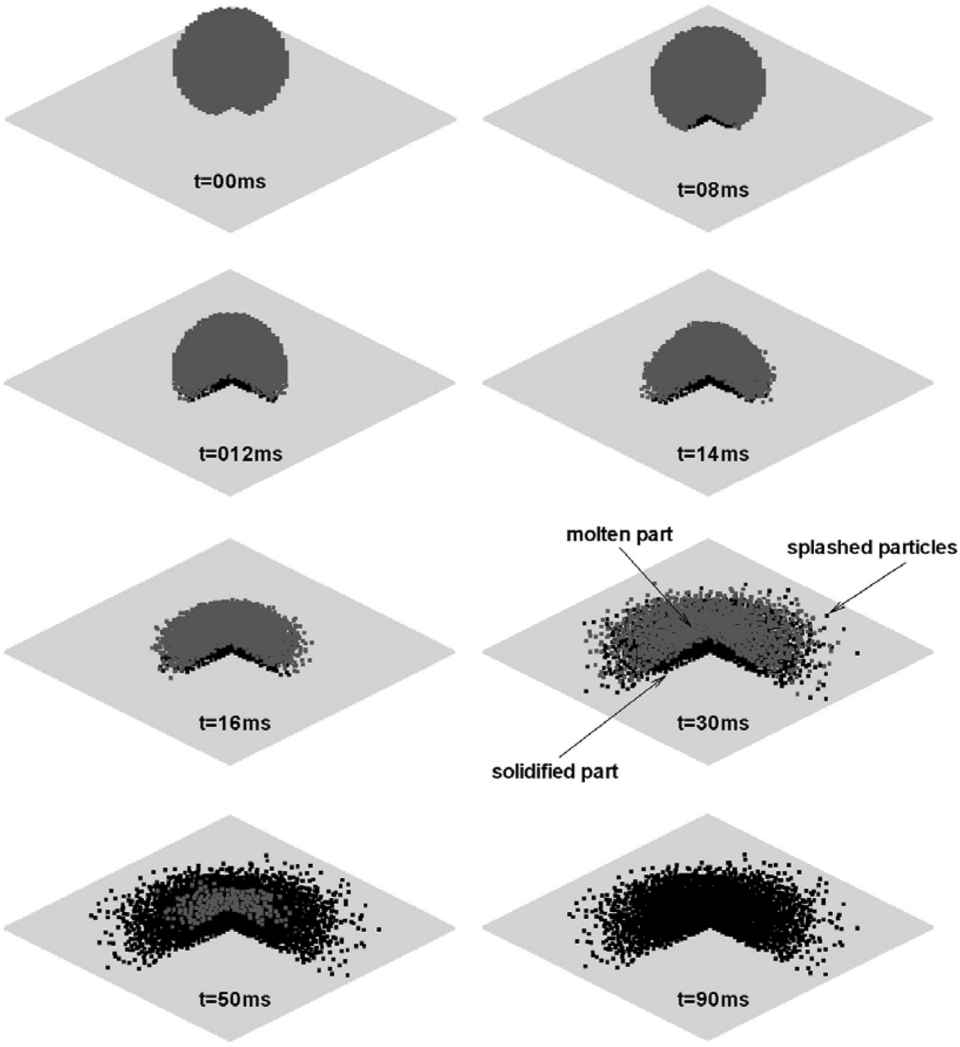

Figure 11. Droplet spreading and solidification on a cold substrate for $\mathrm{Re} = 10$ and $\mathrm{Fr} = 0.2$ at $t = 0$, 8, 12, 14, 16, 30, 50, and 90 ms. The black particles represent solid and the gray particles represent liquid.

5. CONCLUSION

The SPH model has been improved and extended to study the free surface deformation and solidification interface movement. Because of the adaptive nature of the particle interpolation, the SPH model can handle large deformation and movement of multiple interfaces naturally. The SPH method has been applied to study droplet impact on both smooth and rough substrates. The new treatment has been developed to handle particles near the free surface and at the solidification interface. Simulation results show that oxide located uniformly on the droplet surface will be piled up at the region near the advancing fronts when the advancing

contact angle is greater than 90°. The droplet detachment and free surface breakup occur at the outer edge during impact on the rough substrates with roughness average of 62.5 μm and 100 μm, respectively. Numerical results also showed that the rough substrate and solidification will retard the droplet spreading. The capability of the SPH method for simulating problems with both free surface and solidification has been demonstrated for the first time. This SPH method provides a powerful tool to study splat formation and oxide redistribution during droplet impact.

REFERENCE

1. H. B. Xiong, L. L. Zheng, and T. Streibl, A Critical Assessment of Particle Temperature Distribution During Plasma Spraying: Numerical Studies for YSZ, *Plasma Chem. Plasma Process.*, vol. 26, no. 1, pp. 53–72, 2006.
2. L. Li, A. Vaidya, S. Sampath, H. B. Xiong, and L. L. Zheng, Particle Characterization and Splat Formation of Plasma Sprayed Zirconia. *J. Thermal Spray Technol.*, vol. 15, no. 1, pp. 97–105, 2006.
3. H. B. Xiong, L. L. Zheng, L. L., and A. Vaiday, Melting and Oxidation Behavior of In-flight Particles in Plasma Spray Process, *Int. J. Heat Mass Transfer*, vol. 48, pp. 5121–5133, 2005.
4. H. Zhang, X. Y. Wang, L. L. Zheng, and S. Sampath, Numerical Simulation of Nucleation, Solidification and Microstructure Formation in Thermal Spraying, *Int. J. Heat Mass Transfer*, vol. 47, pp. 2191–2203, 2004.
5. H. Zhang, Theoretical Analysis of Spreading and Solidification of Molten Droplet During Thermal Spray Deposition, *Int. J. Heat Mass Transfer*, vol. 42, pp. 2499–2508, 1999.
6. M. Pasandideh-Fard, S. Chandra, and J. Mostaghimi, A Three-Dimensional Model of Droplet Impact and Solidification, *Int. J. Heat Mass Transfer*, vol. 45, pp. 2229–2242, 2002.
7. M. Raessi and J. Mostaghimi, Three-Dimensional Modeling of Density Variation due to Phase Change in Complex Free Surface Flows, *Numer. Heat Transfer B*, vol. 47, pp. 507–531, 2005.
8. L. L. Zheng and H. Zhang, An Adaptive Level Set Method for Moving-Boundary Problems: Applications to Droplet Spreading and Solidification, *Numer. Heat Transfer B*, vol. 37, pp. 435–454, 2000.
9. H. Zhang, L. L. Zheng, V. Prasad, and T. Y. Hou, A Curvilinear Level Set Formulation for Highly Deformable Free Surface Problems with Application to solidification, *Numer. Heat Transfer B*, vol. 34, pp. 1–20, 1998.
10. Z. Zhao, D. Poulikakos, and J. Fukai, Heat Transfer and Fluid Dynamics During the Collision of a Liquid Droplet on a Substrate—I. Modeling, *Int. J. Heat Mass Transfer*, vol. 39, pp. 2771–2789, 1996.
11. V. Butty, D. Poulikakos, and J. Giannakouros, Three-Dimensional Presolidification Heat Transfer and Fluid Dynamics in Molten Microdroplet Deposition, *Int. J. Heat Fluid Flow*, vol. 23, pp. 232–241, 2002.
12. R. A. Gingold and J. J. Monaghan, Smoothed Particle Hydrodynamics—Theory and Application to Non-spherical Stars, *Monthly Notices R. Astron. Soc.*, vol. 181, pp. 375–389, 1977.
13. L. B. Lucy, Numerical Approach to Testing of Fission Hypothesis, *Astron. J.*, vol. 82, pp. 1013–1024, 1977.
14. W. Benz, Smooth Particle Hydrodynamics: A Review, in *Numerical Modeling of Non-linear Stellar Pulsation: Problems and Prospects*, Kluwer, Boston, 1990.

15. J. J. Monaghan, Particle Methods for Hydrodynamics, *Comput. Phys. Rep.*, vol. 3, pp. 71–124, 1985.
16. J. J. Monaghan, Smoothed Particle Hydrodynamics, *Annu. Rev. Astron. Astrophys.*, vol. 30, pp. 543–574, 1992.
17. G. R. Liu and M. B. Liu, *Smoothed Particle Hydrodynamics—A Meshfree Particle Method*, World Scientific, Singapore, 2003.
18. J. P. Morris, Simulating Surface Tension with Smoothed Particle Hydrodynamics, *Int. J. Numer. Meth. Fluids*, vol. 33, pp. 333–353, 2000.
19. S. Nugent and H. A. Posch, Liquid Drops and Surface Tension with Smoothed Particle Applied Mechanics, *Phys. Rev. E*, vol. 62, pp. 4968–4975, 2000.
20. Y. Melean, L. D. G. Sigalotti, and A. Hasmy, On the SPH Tensile Instability in Forming Viscous Liquid Drops, *Comput. Phys. Commun.*, vol. 157, pp. 191–200, 2004.
21. Y. Melean and L. D. G. Sigalotti, Coalescence of Colliding van der Waals Liquid Drops, *Int. J. Heat Mass Transfer*, vol. 48, pp. 4041–4061, 2005.
22. J. J. Monaghan, H. E. Huppert, and M. G. Worster, Solidification Using Smoothed Particle Hydrodynamics, *J. Comput. Phys.*, vol. 206, pp. 684–705, 2005.
23. J. P. Morris, P. J. Fox, and Y. Zhu, Modeling Low Reynolds Number Incompressible Flows Using SPH, *J. Comput. Phys.*, vol. 136, pp. 214–226, 1997.
24. J. J. Monaghan and J. C. Lattanzio, A Refined Particle Method for Astrophysical Problems, *Astron. Astrophys.*, vol. 149, pp. 135–143, 1985.
25. J. J. Monaghan, Simulating Free Surface Flows with SPH, *J. Comput. Phys.*, vol. 110, pp. 399–406, 1994.
26. S. Deshpande, S. Sampath, and H. Zhang, Mechanisms of Oxidation and Its Role in Microstructural Evolution of Metallic Thermal Spray Coatings—Case Study for Ni–Al, *Surface Coatings Technol.*, vol. 200, pp. 5395–5406, 2006.